catalysts

MDPI

Article

Eco-Friendly TiO_2 Nanoparticles: Harnessing *Aloe Vera* for Superior Photocatalytic Degradation of Methylene Blue

Agnese De Luca [1], Angelantonio De Benedetto [1], Valeria De Matteis [1,2,*,†], Mariafrancesca Cascione [1,2,*,†], Riccardo Di Corato [2,3], Chiara Ingrosso [4], Massimo Corrado [1] and Rosaria Rinaldi [1,2]

[1] Department of Mathematics and Physics "Ennio De Giorgi", University of Salento, Via Arnesano, 73100 Lecce, Italy; agnese.deluca@unisalento.it (A.D.L.); angeloantonio.debenedetto@unisalento.it (A.D.B.); massimo.corrado@unisalento.it (M.C.); ross.rinaldi@unisalento.it (R.R.)
[2] Institute for Microelectronics and Microsystems (IMM), CNR, Via Monteroni, 73100 Lecce, Italy; riccardo.dicorato@cnr.it
[3] Center for Biomolecular Nanotechnologies, Istituto Italiano di Tecnologia (IIT), 73010 Arnesano, Italy
[4] CNR-IPCF S.S. Bari, c/o Department of Chemistry, Università degli Studi di Bari, Via Orabona 4, 70126 Bari, Italy; c.ingrosso@ba.ipcf.cnr.it
* Correspondence: valeria.dematteis@unisalento.it (V.D.M.); mariafrancesca.cascione@unisalento.it (M.C.)
† These authors contributed equally to this work.

Abstract: In recent years, the contamination of aquatic environments by organic chemicals, including dyes such as methylene blue (MB), Congo red, and crystal violet, has become an increasing concern, as has their treatment. In this work, titanium dioxide nanoparticles (TiO_2 NPs) were studied for their photocatalytic performance by measuring the degradation of MB under UV light. TiO_2 NPs were synthesized using two synthetic processes optimized in this study: a green method, namely leveraging the natural properties of Aloe vera leaf extract; and a conventional approach. The resulting NPs were thoroughly characterized using X-rays Diffraction (XRD), Transmission Electron Microscopy (TEM), Scanning Electron Microscopy (SEM), Brunauer–Emmett–Teller (BET), UV–Vis and ζ-potential analysis. The TiO_2 NPs synthesized by the green method demonstrated a degradation efficiency of (50 ± 3)% after 180 min, which was significantly higher than the (16 ± 3)% achieved by NPs synthesized through the conventional route. Moreover, the reaction rate constant for the green-synthesized TiO_2 NPs was found to be approximately five times greater than that of the conventionally synthesized NPs. These results open up a new scenario in the pollution removal strategy research, using resources accessible in nature to synthesize NPs with high photocatalytic activity, which could also be useful for other applications, such as hydrogen production.

Keywords: green titanium dioxide nanoparticles; green synthesis; photocatalytic effects; methylene blue

Citation: De Luca, A.; De Benedetto, A.; De Matteis, V.; Cascione, M.; Di Corato, R.; Ingrosso, C.; Corrado, M.; Rinaldi, R. Eco-Friendly TiO_2 Nanoparticles: Harnessing *Aloe Vera* for Superior Photocatalytic Degradation of Methylene Blue. *Catalysts* **2024**, *14*, 820. https://doi.org/10.3390/catal14110820

Academic Editor: Priscy Alfredo Luque Morales

Received: 1 October 2024
Revised: 11 November 2024
Accepted: 13 November 2024
Published: 13 November 2024

1. Introduction

In recent years, the aquatic environment has been found to be contaminated by organic chemicals such as industrial chemicals, pharmaceuticals and consumer products [1]. These substances are only partially removed through conventional physical and biological wastewater treatment, necessitating the use of additional technologies to eliminate toxic pollutants and biologically recalcitrant compounds [2]. For instance, synthetic dyes, such as congo red, toluidine blue, crystal violet and methylene blue, do not biodegrade easily, so they remain in the environment [3]. Advanced oxidation processes (AOPs) are widely employed for treating various types of wastewaters, often in conjunction with biological treatments [4]. AOPs facilitate the in-situ generation of strong oxidants that enable the oxidation of organic compounds [5]. Different AOPs utilize different mechanisms for organic destruction and can be classified into ozone-based, UV-based, catalytic (cAOP), physical (pAOP) and electrochemical (eAOP) AOPs [6]. Heterogeneous photocatalysis is

the one of the most investigated AOPs [7,8]. It involves the creation of electron–hole pairs through the absorption of photons with energy equal to or greater than the semiconductor bandgap [9]. If electron–hole recombination does not occur, these charge carriers can induce the redox reaction with adsorbed species on the semiconductor surface, producing radical species such as hydroxyl radical, superoxide radical anions, and other reactive oxygen species that facilitate the degradation of pollutants [10].

Among several semiconductors, titanium dioxide (TiO_2) is the most thoroughly investigated due to its properties, such as its chemical and thermal stability, high photoactivity, cost-effectiveness, and low toxicity [11]. TiO_2 exhibits exceptional photocatalytic activity when exposed to UV light. Its wide bandgap allows it to generate electron–hole pairs upon irradiation, which are essential for initiating the oxidation and reduction reactions necessary to degrade organic compounds like methylene blue [12,13]. Most recently, due to the necessity of using UV light for TiO_2 irradiation, much research has been focused on different kinds of photocatalysts in order to develop photocatalytic processes that efficiently utilize the visible light [14–16]. For instance, graphitic carbon nitride (g-C_3N_4) is a material with promising properties to be used as a catalyst for treating contaminants in aqueous solution [17]. However, bare g-C_3N_4 was found to have a low and unsatisfactory photocatalytic efficiency, requiring the use of strategies to increase its photocatalytic activity [18]. Another kind of innovative photocatalyst are MXenes and MXene-based nanomaterials, which exhibit fascinating properties such as the possibility of adjusting morphology and bandgap configuration, large specific surface area and thermal strength [19]. However, current studies have only been limited to $Ti_3C_2T_x$ MXene-based nanocomposites, mostly covering the treatment of only a few dyes, and in addition, an ecotoxicological assessment is still lacking [20]. TiO_2 exhibits many advantages over the broad range of other nanomaterials [21], among which there are the following: the more powerful oxidative power of valence band holes compared to the reducibility of photoinduced electrons; the possibility of producing TiO_2 at an industrial level; the fact that it is easy to obtain, inexpensive, and it can be easily synthesized in the laboratory; and being chemically and photochemically stable, safe and non-toxic [22]. TiO_2 occurs in nature in four polymorphisms: anatase; rutile—both with a tetragonal crystal structure—brookite, with an orthorhombic geometry; and TiO_2(B), the monoclinic phase of titanium dioxide [23]. Anatase and rutile are the most commonly occurred forms [24], finding numerous applications including photocatalysis. Anatase exhibits considerably a higher photocatalytic activity than rutile [25], but the photocatalytic activity of TiO_2 depends on several factors, including phase structure, crystallite size, specific surface area and pore structure [26].

Several strategies can be employed to obtain TiO_2 NPs [27], including sol–gel, hydrothermal, and solvothermal methods. For instance, Collazzo et al. used the hydrothermal method with titanium tetraisopropoxide (TTIP) as a precursor in order to obtain TiO_2 nanopowders with a crystallite size ranging from 9 to 17 nm, depending on the synthesis conditions such as temperature and reaction time [28]. Li et al. prepared nano-TiO_2 powders by sol–gel method using tetra-n-butyl-titanate as precursor, investigating different synthesis parameters such as calcination temperature and pH value, to control the grain size and microstructure of nano-TiO_2 powders [29]. Xu et al. synthesized nano-TiO_2 from Tetrabutyl titanate (n-TBT) [30], obtaining NPs with a homogeneous microstructure and a size of around 10–15 nm through a sol–gel process mediated in reverse microemulsion combined with a solvent thermal technique. Sadek et al. used TTIP to prepare TiO_2 nanopowders with a crystal size of 49.3 nm through the sol–gel method [31]. Currently, the growing use of NPs in various applications has stimulated the development of a more inexpensive and sustainable synthesis approach. In particular, the green approach [32], based on the use of natural source materials, allows the elimination or reduction in the use of chemical reagents and the generation of hazardous substances [33]. Green synthesis can be carried out by means of the use of plants and their extracts as well as the microbes, although the former is considered more stable [34]. Several parts of the plant, such as flowers, roots, seeds, and leaves can be employed to prepare plant extracts, though leaves

are more commonly used. Leaves are rich in biomolecules such as proteins, amino acids, terpenoids, flavonoids, and saponins. These molecules are key elements in the synthesis of NPs because they act as reducing agents and capping agents as stabilizer and redox mediators. Santhoshkumar et al. prepared TiO_2 NPs using $TiO(OH)_2$ as a precursor and the aqueous extract of *Psidium guajava* leaves [35]. Ahmad et al. synthesized spherical TiO_2 NPs ranging from 20 to 70 nm using TTIP and *Mentha arvensis* leaves extract as a precursor and reducing agent, respectively [36]. Saini et Kumar achieved the green synthesis of TiO_2 NPs, with an average crystallite size of 15.02 nm, by mixing the *Tinospora cordifolia* leaves extract to the precursor, TTIP [37]. *Aloe Vera* leaves are considered a waste product because they are the residues of the pharmaceutical and cosmetic industries, as the result of processes in which only the *Aloe Vera* gel is used, after the mechanical separation from the leaf. Several studies have shown the use of *Aloe Vera* leaves for different applications ranging from catalyst support material [38], energy field [39,40] to nanomedicine [41,42]. However, most works in which *Aloe Vera* leaves extract was used exploit the entire leaf and thus also the gel content [43,44], whereas in the present study, only the outer part of the leaf was used, leaving the gel for other applications.

Indeed, in this context, TiO_2 NPs have been synthesized via both a green route using *Aloe Vera* leaves extract and a conventional route. The properties of the obtained NPs were characterized by different techniques, specifically TEM, SEM, XRD, BET, UV–vis and ζ-potential measurements. Moreover, the photocatalytic activity of NPs was evaluated by the degradation of methylene blue (MB) under UV light, and the effect of the calcination temperature for TiO_2 NPs synthesized by the green route was investigated. MB was chosen because it is a popular cationic dye frequently used for dyeing (clothes, paper, and leathers) and in the textile industry [3] and it is harmful to human health above a certain concentration [45]. Additionally, methylene blue is resistant to biodegradation, meaning it can persist in the environment for extended periods, leading to the long-term contamination of water bodies [46]. It is highly toxic to aquatic life, even at low concentrations, disrupting ecosystems by affecting the health and reproduction of various species [47]. It also absorbs strongly in the visible spectrum, which can block sunlight from penetrating the water, inhibiting photosynthesis in aquatic plants and algae, further disturbing the balance of aquatic ecosystems [3,48]. Moreover, methylene blue can enter the human food chain through contaminated water sources, posing health risks to humans and animals [49,50]. These characteristics make it a significant concern for environmental pollution. The importance of using green synthesis for environmental purposes, as in the case of wastewater treatment, lies in the fact that the problem that has to be solved is an environmental issue, so it is better to reduce the use of chemical reagents for NP synthesis because their use and disposal could also become an environmental threat.

2. Results and Discussion

The findings of this study underscore the potential of green synthesis methods for TiO_2 NP production, namely by enhancing the efficiency of photocatalytic processes for environmental remediation. In particular, we focused on MB, which is considered a potent pollutant. TiO_2 NPs are crucial in the photocatalysis of methylene blue due to their unique properties and effectiveness in breaking down organic pollutants [51,52]. However, synthetic processes require the use of toxic substances and time-consuming equipment. Therefore, the development of environmentally friendly methods to obtain highly efficient TiO_2 NPs is necessary in order to make it a safe option for treating wastewater without introducing additional harmful substances into the environment [32,53]. Green-synthesized TiO_2 NPs are generally considered non-toxic and eco-friendly, as highlighted in recent studies. For instance, several works reported that TiO_2 NPs produced through green synthesis methods show significantly reduced toxicity compared to conventionally synthesized TiO_2 [54,55]. The use of biocompatible capping agents from plant extracts in green synthesis often results in nanoparticles with lower reactivity and minimal ROS generation, which are primary contributors to toxicity in aquatic environments. Furthermore, the

green-synthesized TiO_2 NPs demonstrate negligible bioaccumulation in various organisms, supporting their potential as a safer, eco-friendly alternative [56]. In our work, we obtained TiO_2 NPs from a conventional route and green route using, in the latter case, *Aloe Vera* leaf extract. This plant is widely distributed in the Mediterranean region and is extensively used in the agricultural, biomedical, and cosmetic fields. In the latter case, in particular, the gel found in the leaves is a valuable material often used to produce skin and beauty lotions. On the other hand, the leaf epidermis, which is considered a waste product, contains high concentrations of vitamins, proteins, and polyphenols, and its extract can be used to produce TiO_2 NPs. The biomolecules enriched the extracts acting as reducing and capping agent [44,57]. The possible principle involves the phytochemicals present in *Aloe vera* that reduce titanium salts (i.e., titanium(IV) isopropoxide) to TiO_2 NPs under mild conditions, avoiding the need for harsh chemicals. These biomolecules also stabilize the nanoparticles, controlling their size and morphology. The green synthesis method is eco-friendly, and the *Aloe vera* extract helps produce TiO_2 NPs with enhanced photocatalytic properties due to the presence of these bioactive compounds [58,59].

Then, we proceed to achieve TiO_2 NPs from the two different routes described in the Materials section following the characterization of their physico-chemical properties. Firstly, we investigated TEM analysis (Figure 1) showing that synthesized TiO_2 NPs showed an irregular shape, as also reported in the literature [60–62]. It was observed that the synthesized NPs had a similar size. An average size of (12 ± 3) nm for the TiO_2-chem (Figure 1a,c,e) NPs and an average size of (10 ± 2) nm for the TiO_2-green NPs were estimated (Figure 1b,d,f). However, aggregation phenomena were also observed, which were more evident in the case of TiO_2-green NPs, probably due to the high concentration of organic compounds enriching the leaves extract.

In order to better analyze the morphologic characteristics of the two types of NPs, SEM analysis was performed. In Figure 2a,b TiO_2-chem NPs and TiO_2-green NPs were reported, respectively. The SEM images derived from chemical approach showed a spherical shaped morphology confirming the TEM acquisition. The TiO_2-green NPs were more aggregated for the presence of organic materials. The EDS spectra confirmed the presence of Ti and O (Figure 2c,d).

Both synthesized TiO_2 NPs showed a negative surface charge in ultrapure water at neutral pH. ζ-potential values of (−18.2 ± 0.2) mV and (−28.4 ± 0.9) mV were observed for TiO_2-chem and TiO_2-green NPs, respectively. Therefore, the adsorption of MB is expected to be favored on the surface of the synthesized NPs, since MB is a cationic dye [63,64].

In addition, since the photocatalytic activity is strictly correlated to the surface area, we performed this measure in order to add more information in evaluating the efficiency of photocatalytic TiO_2-chem and TiO_2-green NPs.

The values of the specific surface area from both types of NPs calculated from the BET method are reported in Table 1. The BET specific surface area of TiO_2-chem NPs was estimated to be 63.2 m^2/g. This value increased in TiO_2-green NPs (70.2 m^2/g).

Table 1. BET surface area of TiO_2-chem and TiO_2-green NPs.

Catalyst	BET Surface Area (m^2/g)
TiO_2-chem NPs	63.2
TiO_2-green NPs	70.2

A larger surface area, typically associated with smaller particles or a porous structure, provides more active sites available for the adsorption of pollutant or reagent molecules. This increase in active sites tends to enhance photocatalytic efficiency, as more molecules can interact with the photogenerated charges (electrons and holes) produced by irradiation.

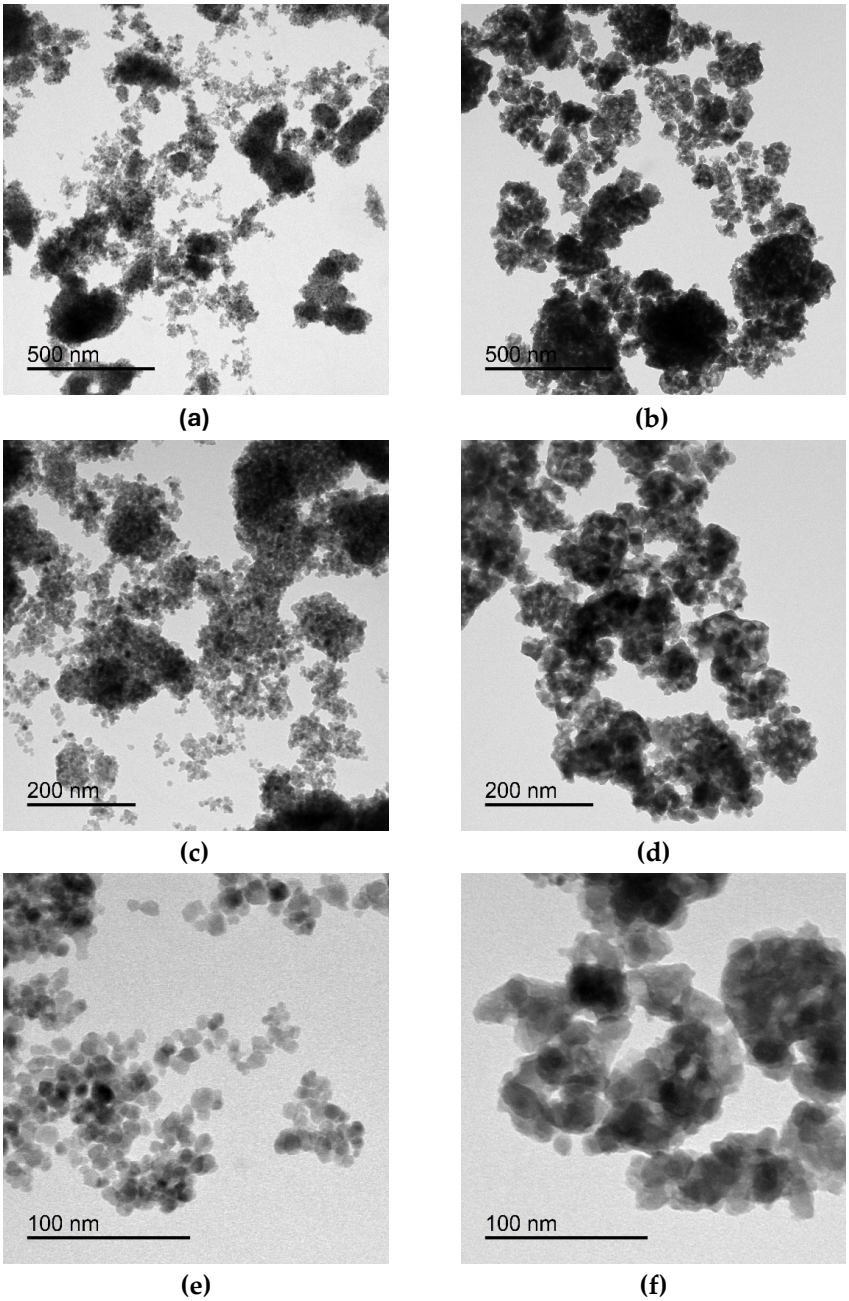

Figure 1. Representative TEM images of TiO_2-chem NPs on the left (**a**,**c**,**e**), TiO_2-green NPs on the right (**b**,**d**,**f**).

The UV characterization showed a pronounced absorption peak at a wavelength of 335 nm from both types of TiO_2 NPs (Figure 3 left). The optical behavior of NPs was investigated using the diffuse reflectance spectrum (Figure 3 right). The spectrum at 385 nm indicates the coordinated electronic transition between the O 2p state and the Ti 3d state. During the green approach, the colloidal solution changed color from white to yellowish-gray, indicating the formation of NPs. The white solution indicated the formation of TiO_2 during the process. The absorption peak was associated with changes in the crystalline phase and the average crystalline size. Consequently, the investigated NP is suitable for catalytic applications. The absorption peak around the 385–400 nm region confirmed the formation of TiO_2 NPs, while the reflectance spectra were consistent with previous studies [59,65].

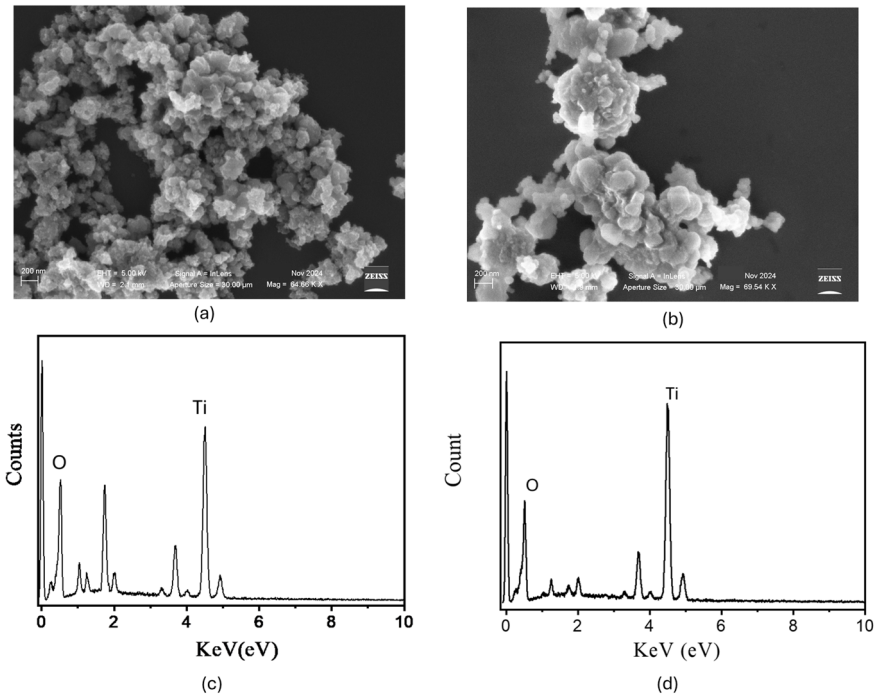

Figure 2. SEM images of TiO_2NPS chem (**a**) and green (**b**). EDS spectra of TiO_2NP_S-chem (**c**) and TiO_2NP_S-green (**d**).

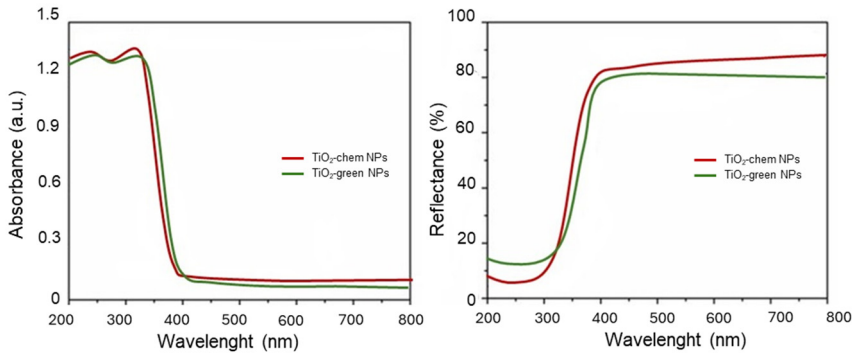

Figure 3. UV–Vis absorbance (**left**) and reflectance spectrum (**right**) of TiO_2-chem NPs (red line) and TiO_2-green NPs (green line).

The optical band gap can be calculated from the Kubelka–Munk method using Tauc relation on reflectance spectra according to [66] (Table 2).

Table 2. Band gap values.

Catalyst	Band Gap (eV)
TiO_2-green NPs	3.1
TiO_2-chem NPs	3.3

These results were interesting, since the lower band gap for TiO_2-green NPs means a good photocatalytic behavior with respect to TiO_2-chem NPs.

The XRD pattern of the synthesized TiO_2 NPs (Figure 4) showed characteristic peaks of anatase for both TiO_2-chem and TiO_2-green NPs around the following 2θ values: 25.4° (101), 37.9° (004), 48.1° (200), 62.9° (204). Two small characteristic peaks of rutile phase, around 27.5° (110) and 36.2° (110), were only observed for the TiO_2-green NPs [67,68]. In addition, a small peak at around 30.8° (121), which can be related to the brookite phase [69], was also observed for both TiO_2 NPs. The anatase phase generally has a higher photocatalytic

performance than that of rutile due to a higher density of localized states and consequent surface-adsorbed hydroxyl radicals and lower recombination of photogenerated electrons and holes in anatase than in rutile [70].

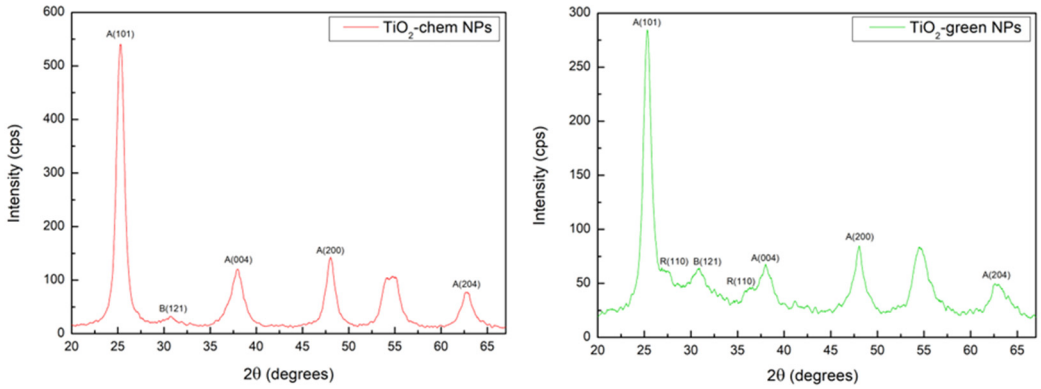

Figure 4. XRD pattern of TiO_2-chem NPs (on the **left**) and TiO_2-green NPs (on the **right**).

After TiO_2 characterization, we performed the assessment of their photocatalytic activity. The photocatalytic activity of the synthesized TiO_2 NPs was evaluated by the degradation of MB in aqueous solution under UV light (Figure 5, upper image). As shown in a lower image of Figure 5, it was found that the kinetics of the photocatalytic degradation follow a pseudo-first-order model (Equation (1)):

$$ln\left(\frac{C_t}{C_0}\right) = -k \cdot t \quad (1)$$

where C_t is the concentration of MB at time t, C_0 is the concentration of MB at time $t = 0$ and k is the reaction rate constant. The reaction rate constant for TiO_2-green NPs was about five times higher than that for TiO_2-chem NPs. As shown in Table 1, the reaction rate constants were 0.004 min^{-1} and 0.0008 min^{-1} for TiO_2-green and TiO_2-chem NPs, respectively. The degradation efficiency was calculated using the following Equation (2):

$$Degradation\ efficiency(\%) = \left(\frac{C_0 - C_t}{C_0}\right) \cdot 100 \quad (2)$$

where C_0 is the concentration of MB at time $t = 0$ and C_t is the concentration of MB at time t.

The general mechanism of degradation is that the generated reactive oxygen species ($^{\bullet}OH$, $O_2^{\bullet -}$, and others) are highly oxidative and can attack the MB molecules, breaking down their chromophore structures and ultimately mineralizing them into CO_2, H_2O, and other less harmful by-products.

This degradation efficiency was obtained using a TiO_2 NPs concentration of 0.4 g/L that is lower than the concentration used in other works, such as in the study carried out by Arvind et al., in which 100 mg of TiO_2 NPs in 100 mL MB solution were used [65]. In addition, only 2 UV lamps of 8 W were used in the irradiation, differently from many other studies [71–73].

As shown in Table 3, the TiO_2-green NPs showed higher efficiency for MB degradation than the TiO_2-chem NPs. In fact, the degradation efficiency values obtained after 180 min were (50 ± 3)% and (16 ± 3)% for TiO_2-green and TiO_2-chem NPs, respectively.

Table 3. Degradation values after 180 min and reaction rate constants for TiO_2 NPs synthesized by green route (TiO_2-green NPs) and by conventional route (TiO_2-chem NPs).

Catalyst	Degradation After 180 min	k
TiO_2-green NPs	(50 ± 3)%	0.004 min^{-1}
TiO_2-chem NPs	(16 ± 3)%	0.0008 min^{-1}

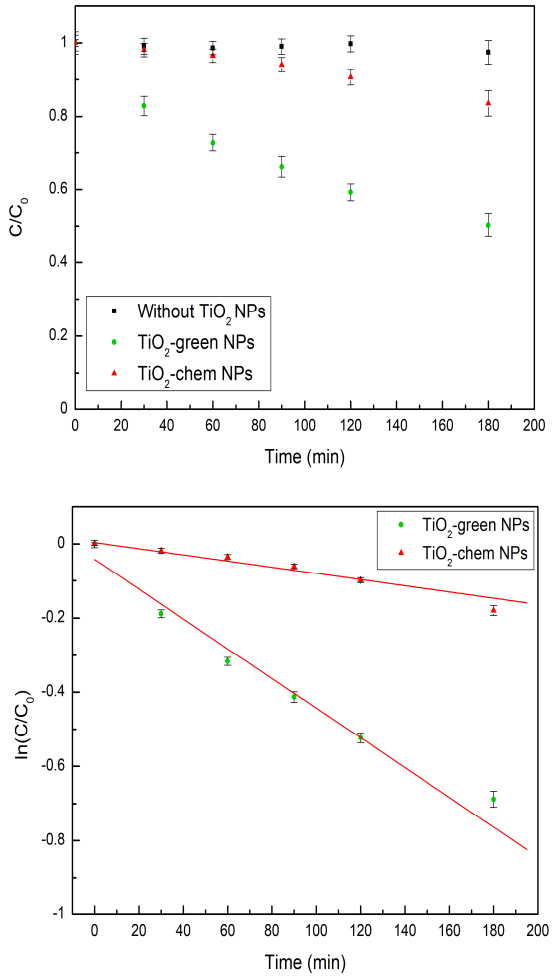

Figure 5. Photocatalytic degradation of MB as a function of time under UV light (**upper** image) and pseudo first-order kinetics (**lower** image). The slope of the fitted lines gave the values of the reaction rate constants: 0.004 min^{-1} (R^2 = 0.97) for TiO_2-green NPs (green circles) and 0.0008 min^{-1} (R^2 = 0.95) for TiO_2-chem NPs (red triangles).

The higher negative ζ-potential value of TiO_2-green NPs, compared with TiO_2-chem NPs, may suggest an improvement in the adsorption of cationic organic pollutants leading to an enhancement of photocatalytic efficiency [74]. Moreover, the small rutile content found for TiO_2-green NPs may indicate that the enhancement of the photocatalytic activity may also be due to charge transfer effects in mixed-phase TiO_2 (anatase/rutile) that improve the charge separation of photogenerated carriers [75,76].

The effect of calcination temperature on TiO_2-green NPs was also analyzed by the evaluation of the photocatalytic activity of the synthesized NPs. As shown in Figure 6, it was observed that the TiO_2-green NPs calcined at 500 °C showed a higher degradation efficiency than the TiO_2 NPs calcined at 400° C. This can be due to the residual organic material on the surface of NPs calcined at 400 °C. The degradation efficiency values obtained after 180 min were (50 ± 3)% for the TiO_2 NPs calcined at 500 °C and (10 ± 4)% for the TiO_2 NPs calcined at 400 °C. A fine white powder was obtained by calcination process at 500 °C, whereas a grey powder with large grains was observed for TiO_2 NPs calcined at 400° C, which may be due to residual carbon from the organic compounds of the leaves extract. The excess residual carbon material on the surface of NPs calcined at 400 °C can cover part of the photocatalyst, leading to an impediment to light access and reactants' access to the photocatalyst surface [77], resulting in a decreased photocatalytic efficiency.

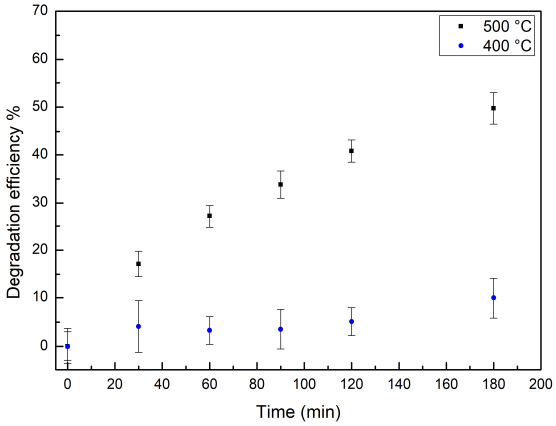

Figure 6. Photocatalytic degradation of MB under UV light: degradation efficiency as a function of time using TiO_2-green NPs calcined at 500 °C (black squares) and calcined at 400 °C (blue circles).

3. Materials and Methods

3.1. Reagents

Titanium (IV) isopropoxide (TTIP, 97%), ethanol absolute (≥99.8%), 2-propanol (≥99.8%), nitric acid (HNO_3 65%), ultrapure water (produced by Barnstead Smart2Pure water purification system Thermo Scientific), and methylene blue hydrate.

3.2. Synthesis of TiO_2 NPs

3.2.1. Conventional Route for Synthesis of TiO_2 NPs (TiO_2-Chem NPs)

TiO_2 NPs were synthesized following the method described in [78] by sol–gel route. Herein, 1 mL of TTIP was slowly added to 5 mL of 25% (v/v) ethanol aqueous solution. The mixture was kept under stirring for 60 min, then the pH was adjusted to 2–3 by adding nitric acid and it was kept under stirring for 60 min. Afterwards, the mixture was dried in an oven using two steps: 120 °C for 120 min and then at 270 °C for 24 h. Finally, the obtained TiO_2 NPs were ground with a mortar. In Figure 7 (on the left), the flow chart of the synthesis process is shown.

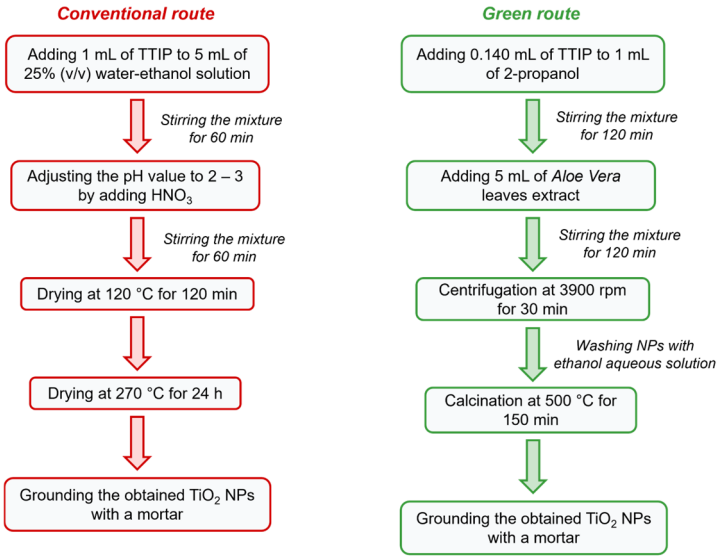

Figure 7. Flow charts concerning the synthesis of TiO_2 NPs: conventional route (on the **left**) and green route (on the **right**).

3.2.2. Green Synthesis of TiO_2 NPs (TiO_2-Green NPs)

Preparation of the Leaves Extract

Aloe vera leaves were separated from the gel and washed with ultrapure water. After drying at room temperature, they were cut into small pieces. Then, 25 g of leaves were transferred into a glass flask containing 250 mL of ultrapure water and the mixture was boiled at 100 °C for 20 min. After cooling, the mixture was filtered by a Whatman filter.

Synthetic Procedure

Here, 0.140 mL of TTIP was slowly added to 1 mL of 2-propanol and the solution was kept under stirring for 120 min. Then, 5 mL of the *Aloe vera* leaves extract were slowly added to the solution and the obtained mixture was kept under stirring for 120 min. Afterwards, TiO_2 NPs were collected by centrifugation at 3900 rpm for 30 min. The collected NPs were washed 4–5 times with 50% (*v*/*v*) ethanol aqueous solution, then the TiO_2 NPs were calcined at 500 °C (or at 400 °C) for 150 min. Lastly, the TiO_2 NPs were ground with a mortar. The flow chart the synthesis process is shown in Figure 7 (on the right).

3.3. Characterization of TiO_2 NPs

TEM characterizations were performed by a JEOL JEM-1011 transmission electron microscope operating at 100 kV. For both synthesized TiO_2 NPs, samples were prepared by dropping a dilute suspension of TiO_2 NPs in ultrapure water on TEM grid and drying overnight at room temperature. ζ-potential analysis was performed at 25 °C by Zetasizer Nano-ZS (Model ZEN3600, Malver Instruments Ltd., Malvern, UK) equipped with a HeNe laser working at 663 nm. Each suspension of TiO_2 NPs (0.4 mg/mL) in ultrapure water was prepared for the measurements. The field emission scanning electron microscopy (FE-SEM) analyses of the samples were performed by using a Zeiss Sigma microscope (Carl Zeiss Co., Oberkochen, Germany) operating at 2–5 kV and equipped with an in-lens secondary electron detector and an INCA Energy Dispersive Spectroscopy (EDS) detector. All the specimens were fixed onto silicon slides that were mounted onto stainless-steel sample holders by using a double-side carbon. For the surface area of the synthesized nanoparticles, a Smart Sorb 92/93 was used. The samples were degassed at 100 °C under nitrogen flow for 90 min before the determination of their surface area. UV–vis analysis spanning the spectral range of 300 ÷ 800 nm was conducted at room temperature using a Varian Cary 5 spectrophotometer (ZEN3600, Malvern Instruments Ltd., Malvern, UK) equipped with a quartz cuvette having a 10 mm path length. Photoluminescence (PL) spectra were measured using FLS1000 photoluminescence spectrometer.

X-ray diffraction analysis was performed in Bragg–Brentano reflection geometry using filtered Cu-Ka radiation. The X-ray diffraction data were collected at a scanning rate of 0.02 degrees per second in 2θ ranging from 20° to 80° by step scanning.

3.4. Assessment of Photocatalytic Activity

The photocatalytic activity of the synthesized TiO_2 NPs was evaluated by the degradation of MB in aqueous solution. With this aim, an UV irradiator (Figure 8), equipped with 2 UV lamps (8 W, λ = 365 nm) and a magnetic stirrer, was used. A suspension of the TiO_2 NPs with a concentration of 0.4 g/L was prepared in 5 mg/L MB solution and it was homogenized by sonication for 60 s. The suspension was kept under stirring and under dark conditions for 30 min to achieve the adsorption–desorption equilibrium, then it was exposed to UV light under stirring condition at a distance from the UV source of about 12.5 cm and samples were taken at different times: 0 min, 30 min, 60 min, 90 min, 120 min, and 180 min. Afterwards, the collected samples were centrifuged in order to remove the nanoparticles and the absorption spectra of the samples were acquired by BioTek Synergy Mx multi-mode microplate reader. The absorption maximum at 664 nm was used to monitor the dye degradation over time.

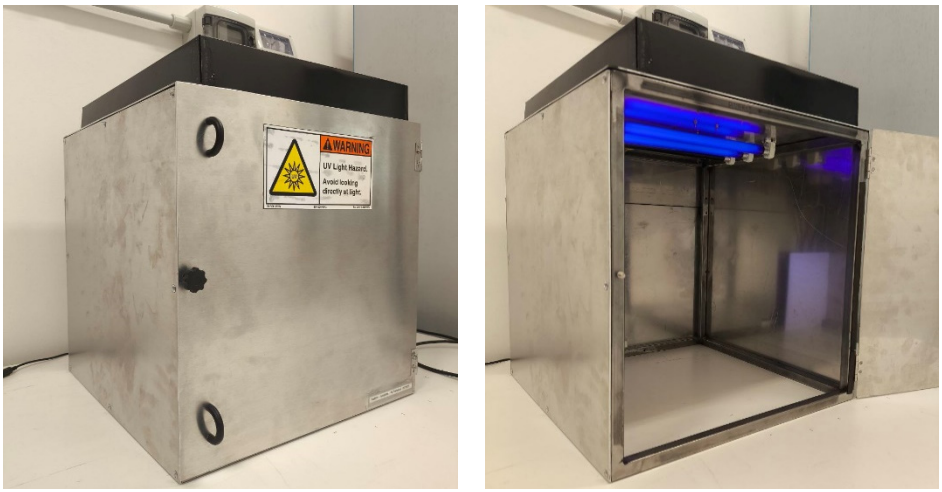

Figure 8. Pictures of the UV irradiator used for photocatalysis experiments.

4. Conclusions

In this work, the photocatalytic activity of TiO_2 NPs synthesized through two synthesis methods, conventional and green, was evaluated by the degradation of MB in aqueous solution, under UV light. Both types of TiO_2 NPs, that appear aggregated from TEM images, showed characteristic peaks of anatase and rutile phase, and TiO_2-green NPs also showed a small peak that can be related to the brookite phase. ζ-potential analysis showed that both synthesized TiO_2 NPs had a negative surface charge at a neutral pH, with a higher negative value of TiO_2-green NPs compared with TiO_2-chem NPs. Concerning the evaluation of the photocatalytic activity by the degradation of MB in aqueous solution, the reaction rate constant for TiO_2-green NPs was about five times higher than that for TiO_2-chem NPs. In fact, the degradation efficiency values obtained after 180 min were (50 ± 3)% for TiO_2-green NPs and (16 ± 3)% for TiO_2-chem NPs. The higher photocatalytic activity exhibited by TiO_2-green NPs compared with TiO_2-chem NPs may be due to the presence of both anatase and rutile phases, which may lead to charge transfer effects that improve the charge separation of photogenerated carriers. Also, the likely introduction of defects or dopants into the TiO_2 lattice by the green synthesis method may create localized energy states that facilitate charge separation and reduce electron–hole recombination. In addition, the higher negative surface charge of TiO_2-green NPs in comparison with TiO_2-chem NPs may lead to the better adsorption of cationic organic pollutants, leading to further enhancement in photocatalytic activity.

Author Contributions: V.D.M. and M.C. (Mariafrancesca Cascione), conceptualization, methodology, supervision, data analysis, editing draft of manuscript; A.D.L., synthesized the nanomaterials; A.D.B. and A.D.L., methodology, writing—original manuscript preparation; R.D.C. and C.I., methodology and data analysis; M.C. (Massimo Corrado), methodology; R.R., funding and supervision. All authors have read and agreed to the published version of the manuscript.

Funding: V.D.M. kindly acknowledges Programma Operativo Nazionale (PON) Ricerca e Innovazione 2014–2020 Azione IV.6 "Contratti su tematiche green"-DM 1062/2021 for sponsoring her salary and work.

Data Availability Statement: The data presented in this study are available in this article.

Conflicts of Interest: There are no conflicts to declare.

References

1. Huerta-Fontela, M.; Galceran, M.T.; Ventura, F. Fast liquid chromatography–quadrupole-linear ion trap mass spectrometry for the analysis of pharmaceuticals and hormones in water resources. *J. Chromatogr. A* **2010**, *1217*, 4212–4222. [CrossRef] [PubMed]
2. Andreozzi, R.; Caprio, V.; Insola, A.; Marotta, R. Advanced oxidation processes (AOP) for water purification and recovery. *Catal. Today* **1999**, *53*, 51–59. [CrossRef]

3. Oladoye, P.O.; Ajiboye, T.O.; Omotola, E.O.; Oyewola, O.J. Methylene blue dye: Toxicity and potential elimination technology from wastewater. *Results Eng.* **2022**, *16*, 100678. [CrossRef]
4. Deng, Y.; Zhao, R. Advanced Oxidation Processes (AOPs) in Wastewater Treatment. *Curr. Pollut. Rep.* **2015**, *1*, 167–176. [CrossRef]
5. Bolton, J.R.; Bircher, K.G.; Tumas, W.; Tolman, C.A. Figures-of-merit for the technical development and application of advanced oxidation technologies for both electric- and solar-driven systems (IUPAC Technical Report). *Pure Appl. Chem.* **2001**, *73*, 627–637. [CrossRef]
6. Miklos, D.B.; Remy, C.; Jekel, M.; Linden, K.G.; Drewes, J.E.; Hübner, U. Evaluation of advanced oxidation processes for water and wastewater treatment—A critical review. *Water Res.* **2018**, *139*, 118–131. [CrossRef]
7. Zhang, Y.; Zhou, B.; Chen, H.; Yuan, R. Heterogeneous photocatalytic oxidation for the removal of organophosphorus pollutants from aqueous solutions: A review. *Sci. Total. Environ.* **2023**, *856*, 159048. [CrossRef]
8. Wang, H.; Li, X.; Zhao, X.; Li, C.; Song, X.; Zhang, P.; Huo, P. A review on heterogeneous photocatalysis for environmental remediation: From semiconductors to modification strategies. *Chin. J. Catal.* **2022**, *43*, 178–214. [CrossRef]
9. Martín, S.S.; Rivero, M.J.; Ortiz, I. Unravelling the Mechanisms that Drive the Performance of Photocatalytic Hydrogen Production. *Catalysts* **2020**, *10*, 901. [CrossRef]
10. Pelaez, M.; Nolan, N.T.; Pillai, S.C.; Seery, M.K.; Falaras, P.; Kontos, A.G.; Dunlop, P.S.M.; Hamilton, J.W.J.; Byrne, J.A.; O'Shea, K.; et al. A review on the visible light active titanium dioxide photocatalysts for environmental applications. *Appl. Catal. B Environ.* **2012**, *125*, 331–349. [CrossRef]
11. Shinnur, M.V.; Pedeferri, M.; Diamanti, M.V. Properties and photocatalytic applications of black TiO_2 produced by thermal or plasma hydrogenation. *Curr. Res. Green Sustain. Chem.* **2024**, *8*, 100415. [CrossRef]
12. Srinivasan, M.; White, T. Degradation of Methylene Blue by Three-Dimensionally Ordered Macroporous Titania. *Environ. Sci. Technol.* **2007**, *41*, 4405–4409. [CrossRef] [PubMed]
13. Abdellah, M.; Nosier, S.; El-Shazly, A.; Mubarak, A. Photocatalytic decolorization of methylene blue using TiO_2/UV system enhanced by air sparging. *Alex. Eng. J.* **2018**, *57*, 3727–3735. [CrossRef]
14. Zou, Z.; Ye, J.; Sayama, K.; Arakawa, H. Direct splitting of water under visible light irradiation with an oxide semiconductor photocatalyst. *Nature* **2001**, *414*, 625–627. [CrossRef]
15. Tsuji, I.; Kato, H.; Kudo, A. Visible-Light-Induced H_2 Evolution from an Aqueous Solution Containing Sulfide and Sulfite over a ZnS–$CuInS_2$–$AgInS_2$ Solid-Solution Photocatalyst. *Angew. Chem. Int. Ed.* **2005**, *44*, 3565–3568. [CrossRef]
16. Shang, M.; Wang, W.; Sun, S.; Zhou, L.; Zhang, L. Bi_2WO_6 Nanocrystals with High Photocatalytic Activities under Visible Light. *J. Phys. Chem. C* **2008**, *112*, 10407–10411. [CrossRef]
17. Xiao, H.; Wang, W.; Liu, G.; Chen, Z.; Lv, K.; Zhu, J. Photocatalytic performances of g-C3N4 based catalysts for RhB degradation: Effect of preparation conditions. *Appl. Surf. Sci.* **2015**, *358*, 313–318. [CrossRef]
18. Chang, F.; Xie, Y.; Li, C.; Chen, J.; Luo, J.; Hu, X.; Shen, J. A facile modification of g-C_3N_4 with enhanced photocatalytic activity for degradation of methylene blue. *Appl. Surf. Sci.* **2013**, *280*, 967–974. [CrossRef]
19. Zhan, X.; Si, C.; Zhou, J.; Sun, Z. MXene and MXene-based composites: Synthesis, properties and environment-related applications. *Nanoscale Horiz.* **2020**, *5*, 235–258. [CrossRef]
20. Im, J.K.; Sohn, E.J.; Kim, S.; Jang, M.; Son, A.; Zoh, K.-D.; Yoon, Y. Review of MXene-based nanocomposites for photocatalysis. *Chemosphere* **2021**, *270*, 129478. [CrossRef]
21. Armaković, S.J.; Savanović, M.M.; Armaković, S. Titanium Dioxide as the Most Used Photocatalyst for Water Purification: An Overview. *Catalysts* **2022**, *13*, 26. [CrossRef]
22. Lee, S.-Y.; Park, S.-J. TiO_2 photocatalyst for water treatment applications. *J. Ind. Eng. Chem.* **2013**, *19*, 1761–1769. [CrossRef]
23. Ma, Y.; Wang, X.; Jia, Y.; Chen, X.; Han, H.; Li, C. Titanium Dioxide-Based Nanomaterials for Photocatalytic Fuel Generations. *Chem. Rev.* **2014**, *114*, 9987–10043. [CrossRef] [PubMed]
24. Eddy, D.R.; Permana, M.D.; Sakti, L.K.; Sheha, G.A.N.; Solihudin; Hidayat, S.; Takei, T.; Kumada, N.; Rahayu, I. Heterophase Polymorph of TiO_2 (Anatase, Rutile, Brookite, TiO_2 (B)) for Efficient Photocatalyst: Fabrication and Activity. *Nanomaterials* **2023**, *13*, 704. [CrossRef] [PubMed]
25. Linsebigler, A.L.; Lu, G.; Yates, J.T. Photocatalysis on TiO_2 Surfaces: Principles, Mechanisms, and Selected Results. *Chem. Rev.* **1995**, *95*, 735–758. [CrossRef]
26. Yu, J.; Yu, J.C.; Leung, M.K.-P.; Ho, W.; Cheng, B.; Zhao, X.; Zhao, J. Effects of acidic and basic hydrolysis catalysts on the photocatalytic activity and microstructures of bimodal mesoporous titania. *J. Catal.* **2003**, *217*, 69–78. [CrossRef]
27. Mironyuk, I.F.; Soltys, L.M.; Tatarchuk, T.R.; Savka, K.O. Methods of Titanium Dioxide Synthesis (Review). *Phys. Chem. Solid State* **2020**, *21*, 462–477. [CrossRef]
28. Collazzo, G.C.; Jahn, S.L.; Carreño, N.L.V.; Foletto, E.L. Temperature and reaction time effects on the structural properties of titanium dioxide nanopowders obtained via the hydrothermal method. *Braz. J. Chem. Eng.* **2011**, *28*, 265–272. [CrossRef]
29. Li, B.; Wang, X.; Yan, M.; Li, L. Preparation and characterization of nano-TiO_2 powder. *Mater. Chem. Phys.* **2002**, *78*, 184–188. [CrossRef]
30. Xu, H.; Li, M.; Jun, Z. Preparation, characterization, and photocatalytic studies on anatase nano-TiO_2 at internal air lift circulating photocatalytic reactor. *Mater. Res. Bull.* **2013**, *48*, 3144–3148. [CrossRef]
31. Sadek, O.; Touhtouh, S.; Rkhis, M.; Anoua, R.; El Jouad, M.; Belhora, F.; Hajjaji, A. Synthesis by sol-gel method and characterization of nano-TiO_2 powders. *Mater. Today Proc.* **2022**, *66*, 456–458. [CrossRef]

32. Verma, V.; Al-Dossari, M.; Singh, J.; Rawat, M.; Kordy, M.G.M.; Shaban, M. A Review on Green Synthesis of TiO_2 NPs: Photocatalysis and Antimicrobial Applications. *Polymers* **2022**, *14*, 1444. [CrossRef] [PubMed]
33. Anastas, P.T. Green Chemistry and the Role of Analytical Methodology Development. *Crit. Rev. Anal. Chem.* **1999**, *29*, 167–175. [CrossRef]
34. Singh, P.; Kim, Y.-J.; Zhang, D.; Yang, D.-C. Biological Synthesis of Nanoparticles from Plants and Microorganisms. *Trends Biotechnol.* **2016**, *34*, 588–599. [CrossRef]
35. Santhoshkumar, T.; Rahuman, A.A.; Jayaseelan, C.; Rajakumar, G.; Marimuthu, S.; Kirthi, A.V.; Velayutham, K.; Thomas, J.; Venkatesan, J.; Kim, S.-K. Green synthesis of titanium dioxide nanoparticles using Psidium guajava extract and its antibacterial and antioxidant properties. *Asian Pac. J. Trop. Med.* **2014**, *7*, 968–976. [CrossRef] [PubMed]
36. Ahmad, W.; Jaiswal, K.K.; Soni, S. Green synthesis of titanium dioxide (TiO_2) nanoparticles by using *Mentha arvensis* leaves extract and its antimicrobial properties. *Inorg. Nano-Metal Chem.* **2020**, *50*, 1032–1038. [CrossRef]
37. Saini, R.; Kumar, P. Green synthesis of TiO_2 nanoparticles using *Tinospora cordifolia* plant extract & its potential application for photocatalysis and antibacterial activity. *Inorg. Chem. Commun.* **2023**, *156*, 111221. [CrossRef]
38. Dülger, B.; Özkan, G.; Angı, O.S.; Özkan, G. Green synthesis of TiO_2 nanoparticles using Aloe Vera extract as catalyst support material and studies of their catalytic activity in dehydrogenation of Ethylenediamine Bisborane. *Int. J. Hydrogen Energy* **2024**, *75*, 466–474. [CrossRef]
39. Jiang, L.; Zhou, S.; Yang, J.; Wang, H.; Yu, H.; Chen, H.; Zhao, Y.; Yuan, X.; Chu, W.; Li, H. Near-Infrared Light Responsive TiO_2 for Efficient Solar Energy Utilization. *Adv. Funct. Mater.* **2022**, *32*, 2108977. [CrossRef]
40. Guo, Q.; Ma, Z.; Zhou, C.; Ren, Z.; Yang, X. Single Molecule Photocatalysis on TiO_2 Surfaces. *Chem. Rev.* **2019**, *119*, 11020–11041. [CrossRef]
41. Fadeel, D.A.; Hanafy, M.; Kelany, N.; Elywa, M. Novel greenly synthesized titanium dioxide nanoparticles compared to liposomes in drug delivery: In vivo investigation on Ehrlich solid tumor model. *Heliyon* **2021**, *7*, e07370. [CrossRef] [PubMed]
42. De Matteis, V.; Rizzello, L.; Di Bello, M.P.; Rinaldi, R. One-step synthesis, toxicity assessment and degradation in tumoral pH environment of SiO_2@Ag core/shell nanoparticles. *J. Nanopart. Res.* **2017**, *19*, 196.
43. Ahmed, N.K.; Abbady, A.; Elhassan, Y.A.; Said, A.H. Green Synthesized Titanium Dioxide Nanoparticle from Aloe Vera Extract as a Promising Candidate for Radiosensitization Applications. *BioNanoScience* **2023**, *13*, 730–743. [CrossRef]
44. Venkatesh, K.S.; Krishnamoorthi, S.R.; Palani, N.S.; Thirumal, V.; Jose, S.P.; Wang, F.-M.; Ilangovan, R. Facile one step synthesis of novel TiO2 nanocoral by sol–gel method using Aloe vera plant extract. *Indian J. Phys.* **2015**, *89*, 445–452. [CrossRef]
45. Cheng, J.; Zhan, C.; Wu, J.; Cui, Z.; Si, J.; Wang, Q.; Peng, X.; Turng, L.-S. Highly Efficient Removal of Methylene Blue Dye from an Aqueous Solution Using Cellulose Acetate Nanofibrous Membranes Modified by Polydopamine. *ACS Omega* **2020**, *5*, 5389–5400. [CrossRef] [PubMed]
46. Modi, S.; Yadav, V.K.; Gacem, A.; Ali, I.H.; Dave, D.; Khan, S.H.; Yadav, K.K.; Rather, S.-U.; Ahn, Y.; Son, C.T.; et al. Recent and Emerging Trends in Remediation of Methylene Blue Dye from Wastewater by Using Zinc Oxide Nanoparticles. *Water* **2022**, *14*, 1749. [CrossRef]
47. Li, S.; Cui, Y.; Wen, M.; Ji, G. Toxic Effects of Methylene Blue on the Growth, Reproduction and Physiology of *Daphnia magna*. *Toxics* **2023**, *11*, 594. [CrossRef]
48. Moorthy, A.K.; Rathi, B.G.; Shukla, S.P.; Kumar, K.; Bharti, V.S. Acute toxicity of textile dye Methylene blue on growth and metabolism of selected freshwater microalgae. *Environ. Toxicol. Pharmacol.* **2021**, *82*, 103552. [CrossRef]
49. Khan, I.; Saeed, K.; Zekker, I.; Zhang, B.; Hendi, A.H.; Ahmad, A.; Ahmad, S.; Zada, N.; Ahmad, H.; Shah, L.A.; et al. Review on Methylene Blue: Its Properties, Uses, Toxicity and Photodegradation. *Water* **2022**, *14*, 242. [CrossRef]
50. Yahaya, N.P.; Ali, I.; Modu, K.A.; Adamu, S. Adsorption Study of Methylene Blue onto Power Activated Carbon Prepared from Ananas Comosus Peels. *Nanochemistry Res.* **2023**, *8*, 231–242. [CrossRef]
51. Yasin, S.A.; Abbas, J.A.; Ali, M.M.; Saeed, I.A.; Ahmed, I.H. Methylene blue photocatalytic degradation by TiO_2 nanoparticles supported on PET nanofibres. *Mater. Today Proc.* **2019**, *20*, 482–487. [CrossRef]
52. Niu, L.; Zhao, X.; Tang, Z.; Lv, H.; Wu, F.; Wang, X.; Zhao, T.; Wang, J.; Wu, A.; Giesy, J. Difference in performance and mechanism for methylene blue when TiO2 nanoparticles are converted to nanotubes. *J. Clean. Prod.* **2021**, *297*, 126498. [CrossRef]
53. Sethy, N.K.; Arif, Z.; Mishra, P.K.; Kumar, P. Green synthesis of TiO_2 nanoparticles from Syzygium cumini extract for photocatalytic removal of lead (Pb) in explosive industrial wastewater. *Green Process. Synth.* **2020**, *9*, 171–181. [CrossRef]
54. Jafari, A.; Rashidipour, M.; Kamarehi, B.; Alipour, S.; Ghaderpoori, M. Toxicity of green synthesized TiO_2 nanoparticles (TiO_2 NPs) on zebra fish. *Environ. Res.* **2022**, *212*, 113542. [CrossRef] [PubMed]
55. Sagadevan, S.; Imteyaz, S.; Murugan, B.; Lett, J.A.; Sridewi, N.; Weldegebrieal, G.K.; Fatimah, I.; Oh, W.-C. A comprehensive review on green synthesis of titanium dioxide nanoparticles and their diverse biomedical applications. *Green Process. Synth.* **2022**, *11*, 44–63. [CrossRef]
56. Weng, Y.; Bai, X.; Kang, M.; Huang, Y.; Ji, Y.; Wang, H.; Hua, Z. Comparative analysis of chemically and green synthesized titanium dioxide nanoparticles for the regulation of photosynthesis in *Lactuca sativa* L. *Environ. Sci. Nano* **2024**, *11*, 161–174. [CrossRef]
57. De Matteis, V.; Cascione, M.; Rinaldi, R. Titanium dioxide: Antimicrobial surfaces and toxicity assessment. In *Titanium Dioxide (Tio_2) and Its Applications*; Elsevier: Amsterdam, The Netherlands, 2021; pp. 373–393. [CrossRef]

58. Yousef, T.; El-Gammal, O.; Ahmed, S.F.; Abu El-Reash, G. Synthesis, biological and comparative DFT studies on Ni(II) complexes of NO and NOS donor ligands. *Spectrochim. Acta Part A Mol. Biomol. Spectrosc.* **2015**, *135*, 690–703. [CrossRef]
59. Rajkumari, J.; Magdalane, C.M.; Siddhardha, B.; Madhavan, J.; Ramalingam, G.; Al-Dhabi, N.A.; Arasu, M.V.; Ghilan, A.; Duraipandiayan, V.; Kaviyarasu, K. Synthesis of titanium oxide nanoparticles using *Aloe barbadensis* mill and evaluation of its antibiofilm potential against Pseudomonas aeruginosa PAO1. *J. Photochem. Photobiol. B Biol.* **2019**, *201*, 111667. [CrossRef]
60. Pellegrino, F.; Ortel, E.; Mielke, J.; Schmidt, R.; Maurino, V.; Hodoroaba, V.-D. Customizing New Titanium Dioxide Nanoparticles with Controlled Particle Size and Shape Distribution: A Feasibility Study Toward Reference Materials for Quality Assurance of Nonspherical Nanoparticle Characterization. *Adv. Eng. Mater.* **2022**, *24*, 2101347. [CrossRef]
61. Almomen, A.; Alsaleh, N.B.; El-Toni, A.M.; El-Mahrouky, M.A.; Alhowyan, A.A.; Alkholief, M.; Alshamsan, A.; Khurana, N.; Ghandehari, H. In Vitro Safety Assessment of In-House Synthesized Titanium Dioxide Nanoparticles: Impact of Washing and Temperature Conditions. *Int. J. Mol. Sci.* **2023**, *24*, 9966. [CrossRef]
62. Bahri, S.S.; Harun, Z.; Hubadillah, S.K.; Salleh, W.N.W.; Rosman, N.; Kamaruddin, N.H.; Azhar, F.H.; Sazali, N.; Ahmad, R.A.R.; Basri, H. Review on recent advance biosynthesis of TiO_2nanoparticles from plant-mediated materials: Characterization, mechanism and application. *IOP Conf. Ser. Mater. Sci. Eng.* **2021**, *1142*, 012005. [CrossRef]
63. Guillard, C.; Lachheb, H.; Houas, A.; Ksibi, M.; Elaloui, E.; Herrmann, J.-M. Influence of chemical structure of dyes, of pH and of inorganic salts on their photocatalytic degradation by TiO_2 comparison of the efficiency of powder and supported TiO_2. *J. Photochem. Photobiol. A Chem.* **2003**, *158*, 27–36. [CrossRef]
64. Zhang, M.; Shi, L.; Yuan, S.; Zhao, Y.; Fang, J. Synthesis and photocatalytic properties of highly stable and neutral TiO_2/SiO_2 hydrosol. *J. Colloid Interface Sci.* **2009**, *330*, 113–118. [CrossRef] [PubMed]
65. Aravind, M.; Amalanathan, M.; Mary, M.S.M. Synthesis of TiO_2 nanoparticles by chemical and green synthesis methods and their multifaceted properties. *SN Appl. Sci.* **2021**, *3*, 409. [CrossRef]
66. Rashidi, P.; Ghamari, M.; Ghasemifard, M. The structural and optical band gap energy evaluation of nano TiO_2powders by diffuse reflectance spectroscopy prepared via combustion method. *Int. Nano Lett.* **2020**, *10*, 271–277. [CrossRef]
67. De Matteis, V.; Cascione, M.; Toma, C.C.; Pellegrino, P.; Rizzello, L.; Rinaldi, R. Tailoring Cell Morphomechanical Perturbations Through Metal Oxide Nanoparticles. *Nanoscale Res. Lett.* **2019**, *14*, 109. [CrossRef]
68. John, A.K.; Palaty, S.; Sharma, S.S. Greener approach towards the synthesis of titanium dioxide nanostructures with exposed {001} facets for enhanced visible light photodegradation of organic pollutants. *J. Mater. Sci. Mater. Electron.* **2020**, *31*, 20868–20882. [CrossRef]
69. Di Paola, A.; Bellardita, M.; Palmisano, L. Brookite, the Least Known TiO_2 Photocatalyst. *Catalysts* **2013**, *3*, 36–73. [CrossRef]
70. Hanaor, D.A.H.; Sorrell, C.C. Review of the anatase to rutile phase transformation. *J. Mater. Sci.* **2011**, *46*, 855–874. [CrossRef]
71. Nethravathi, P.; Udayabhanu; Nagaraju, G.; Suresh, D. TiO_2 and Ag-TiO_2 nanomaterials for enhanced photocatalytic and antioxidant activity: Green synthesis using Cucumis melo juice. *Mater. Today Proc.* **2022**, *49*, 841–848. [CrossRef]
72. Madadi, Z.; Soltanieh, M.; Lotfabad, T.B.; Nazari, S. Green synthesis of titanium dioxide nanoparticles with Glycyrrhiza glabra and their photocatalytic activity. *Asian J. Green Chem.* **2020**, *4*, 3. [CrossRef]
73. Ngoepe, N.M.; Mathipa, M.M.; Hintsho-Mbita, N.C. Biosynthesis of titanium dioxide nanoparticles for the photodegradation of dyes and removal of bacteria. *Optik* **2020**, *224*, 165728. [CrossRef]
74. Liao, D.; Wu, G.; Liao, B. Zeta potential of shape-controlled TiO2 nanoparticles with surfactants. *Colloids Surf. A Physicochem. Eng. Asp.* **2009**, *348*, 270–275. [CrossRef]
75. Wei, Y.; Tokina, M.V.; Benderskii, A.V.; Zhou, Z.; Long, R.; Prezhdo, O.V. Quantum dynamics origin of high photocatalytic activity of mixed-phase anatase/rutile TiO_2. *J. Chem. Phys.* **2020**, *153*, 044706. [CrossRef] [PubMed]
76. Shen, S.; Wang, X.; Chen, T.; Feng, Z.; Li, C. Transfer of Photoinduced Electrons in Anatase–Rutile TiO_2 Determined by Time-Resolved Mid-Infrared Spectroscopy. *J. Phys. Chem. C* **2014**, *118*, 12661–12668. [CrossRef]
77. Zhang, J.; Vasei, M.; Sang, Y.; Liu, H.; Claverie, J.P. TiO_2@Carbon Photocatalysts: The Effect of Carbon Thickness on Catalysis. *ACS Appl. Mater. Interfaces* **2016**, *8*, 1903–1912. [CrossRef]
78. Leena, M.; Srinivasan, S. Synthesis and ultrasonic investigations of titanium oxide nanofluids. *J. Mol. Liq.* **2015**, *206*, 103–109. [CrossRef]